Applied Catalysis B: Environmental 224 (2018) 204–213

Contents lists available at ScienceDirect

Applied Catalysis B: Environmental

journal homepage: www.elsevier.com/locate/apcatb

A multifunctional graphene-based nanofiltration membrane under photo-assistance for enhanced water treatment based on layer-by-layer sieving

Qi Zhang, Shuo Chen*, Xinfei Fan, Haiguang Zhang, Hongtao Yu, Xie Quan

Key Laboratory of Industrial Ecology and Environmental Engineering (Ministry of Education, China), School of Environmental Science and Technology, Dalian University of Technology, Dalian 116024, China

ARTICLE INFO

Keywords:
Nanofiltration
Multifunctional membrane
Photocatalysis
Enhanced performance
Water treatment

ABSTRACT

Nanofiltration (NF) provides an effective strategy for rejecting large organic molecules. However, attaining high permeability, antifouling ability and good selectivity simultaneously still remains a crucial task for existing NF technologies. Herein, we built a photo-assisted multifunctional NF membrane assembled with g-C_3N_4, TiO_2, carbon nanotubes (CNTs) and graphene oxide (GO), in which CNTs not only expand the interlayer space between neighbored graphene sheets, but also enhance the stability and strength of GO layer. Benefiting from the photo-assistance, our NF membranes show an enhanced water flux (~16 L m^{-2} h^{-1} bar^{-1}), while keep a high dye rejection (~100% for Methyl Orange). The photo-assisted NF membranes also display good rejection ratio for salt ions (i.e., 67% for Na_2SO_4) due to the layer-by-layer sieving. Meanwhile, the NF membrane coupled with photocatalysis exhibits a multifunctional characteristic for the efficient removal of ammonia (50%), antibiotic (80%) and bisphenol A (82%) in water. Besides, the performance of integrated system is also tested by treating the real aquaculture wastewater to evaluate its practical application ability. The lost flux of the fouled membrane is effectively recovered by the photochemically assisted process. Hence, this work mitigates the longstanding challenge of GO-based NF membranes in large-scale application by integrating photocatalysis and nanofiltration technologies.

1. Introduction

Increasingly dwindling water resources have stimulated the development of advanced water treatment technologies that can afford clean and fresh water by the more eco-friendly and energy-saving strategies [1]. Nanofiltration (NF) technology has been widely used in the drinking water and waste water advanced treatments because of its relatively low energy consumption and simple process handling, in which the properties of NF membranes are of vital importance [2]. Graphene oxide (GO) has been reported as attractive materials for developing a novel class of NF membranes with extraordinary separation performance on account of their highly ordered 2D nanochannels between two graphene sheets [3]. Conventional GO-based NF membranes (CGNMs) are relatively effective (rejection > 85%) in nanofiltration process for sieving molecular weights between 200 and 1000 g mol^{-1} due to its pore size around 1 nm, nevertheless it is difficult for CGNMs to reject pollutants with sizes smaller than membrane pores, such as ammonia, antibiotics and endocrine disrupting chemicals which are normally present in the surface water owing to its single separation function [4]. Unfortunately, these pollutants adverse for size exclusion separation seriously threaten the ecological safety and human health even at trace levels because of their persistence, toxicity, and bioaccumulation [5]. Although pressure-driven CGNMs exhibit the potential for the rejection of various charged ions, a trade-off between flux and ions rejection limits their further applications [6]. Meanwhile, the C-GNMs are not effective for the rejection of salt ions (rejection < 50%) [4]. Moreover, CGNMs with low water flux are difficult for achieving large-scale application (< 10 L m^{-2} h^{-1} bar^{-1}) [2,7]. Currently, attaining high flux usually suffers from the high operating pressure in nanofiltration process, which results in a high energy cost. In addition, membrane fouling is also a universal and costly problem for CGNMs that generally causes deterioration in membrane performance, especially decreased permeating flux. Therefore, advances in the design and synthesis of multifunctional NF membranes that not only are able to offer high flux, high retention and good antifouling ability, but also are affordable and convenient for practical application would have tremendous impact in water supply with high quality.

Construction of multifunctional NF membranes depends on the structural tailoring and the introduction of functional layers. Recently, photocatalytic technologies have been extensively used in combination

* Corresponding author.
E-mail address: shuochen@dlut.edu.cn (S. Chen).

http://dx.doi.org/10.1016/j.apcatb.2017.10.016
Received 26 May 2017; Received in revised form 18 September 2017; Accepted 7 October 2017
Available online 07 October 2017

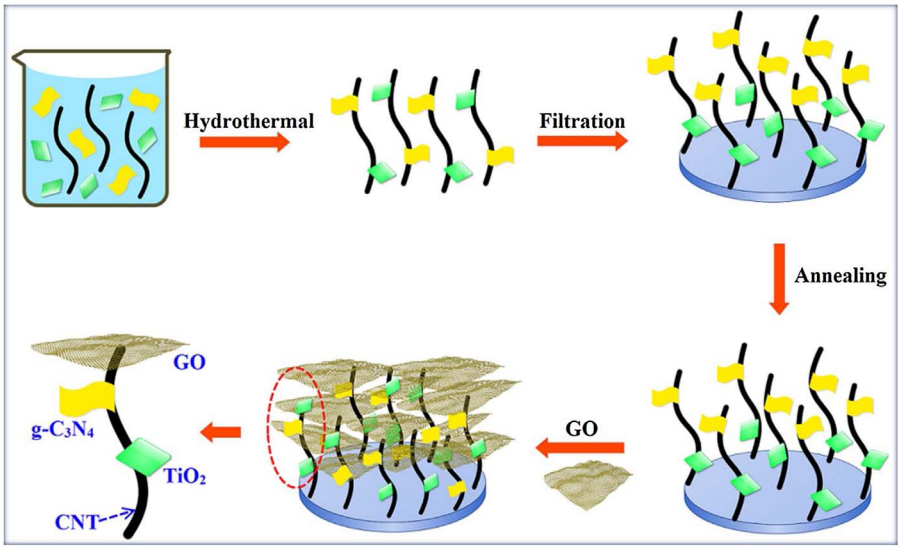

Scheme 1. Schematic illustration of the overall steps used in the preparation of GO/CN/TiO-CNT membranes.

with membrane processes to alleviate membrane fouling and further extend the practical applications of membranes [8–12]. During this integrated process, photocatalytic degradation of organic contaminants that can not be retained by size exclusion separation prevents them from permeating through the membranes. Simultaneously, the inherent membrane fouling is also mitigated due to the efficient decomposition of pollutants by photocatalysis. Based on the mechanism of photo-induced hydrophilicity [13], introducing the photocatalytic technologies into the CGNMs can efficiently enhance the hydrophilia of membrane surface, which is favorable to improving water flux. Generally, Donnan exclusion mechanism is used for explaining the rejection performance of charged CGNMs [14]. The abundant photogenerated charges are generated by the attractive heterostructure of g-C_3N_4 (CN) and TiO_2 (TiO), and these charges on the membranes will increase the rejection of co-ions (ions with the same charge as the membrane) in water according to Donnan theory. If these fascinating photochemical functions can be introduced into CGNMs, the additional photochemical functions will promote the physicochemical functions that are not available by size or charge exclusion alone. This might be an alternative approach to solve the issue of single separation function of CGNMs.

Carbon nanotubes (CNTs) provide a unique 1D nanochannel for water transporting. Intensively theoretical calculations predict that the permeation of water through the CNT is extremely fast [15,16]. And Hinds experimentally proved the water flux through aligned multi-walled CNTs over 4 orders of magnitude larger than conventional hydrodynamic flow prediction [17]. Undoubtedly, aligned CNTs forming a stereochemical structure are fine channels for liquid flowing. Thanks to the low resistivity and mass density, large specific surface area and good chemical stability, CNTs are used as conduits for transporting and storing electrons from photoirradiated photocatalyst [18,19]. In addition, owing to the bridging of CNTs, the interlayer space between neighbored graphene sheets is expanded, which is advantageous to the water flux. Meanwhile, the strong noncovalent π–π interactions between CNTs and GO are also beneficial to enhancing the stability and strength of GO layer.

To effectively make a balance between flux and rejection of NF membranes and overcome the defect of single separation function of CGNMs, we design a multifunctional NF membrane system with both high flux and high rejection by CNTs-bridged the g-C_3N_4/TiO_2 nanosheets and GO layers under photochemical assistance for the first time. Different from the CGNMs, the plentiful photogenerated charges on the membrane forming a reinforced Donnan potential are beneficial to the high ions rejection of membranes. A high water flux is also supposed because of the photoinduced hydrophilicity of g-C_3N_4/TiO_2 relying on the formation of surface defects upon light illumination and Hagen – Poiseuille theory. Meanwhile, the "grafting" of CNTs into the interlayers of GO skin layers and membrane support can increase the interlayer spacing from below one nanometer to several nanometers, which is conducive to the water transporting. Furthermore, the self-assembly of CNTs, thin g-C_3N_4 and TiO_2 nanosheets tends to forming a 3D nanoporous network, contributing to attaining high membrane porosity. The present study provides a new strategy for the design of high-performance multifunctional GO-based NF membranes and also provides a better understanding of the enhanced transport and rejection mechanism of photo-assisted GO-based NF membranes. Besides, the efficient antifouling ability of the GO-base NF membranes is also demonstrated under the photochemical assistance.

2. Experimental

2.1. Assembly of GO/CN/TiO-CNT membrane

100 mg of CN/TiO-CNT photocatalyst (see supporting information) was dispersed in 200 mL pure water (Millipore, 18 MΩ Cm) under assistance of ultrasonification. To obtain the uniform distribution of the nanoporous mat, the dissolved photocatalyst suspensions (50 mL) above were filtrated stepwise (5 mL each time) through the alumina membrane support with the assistance of a vacuum [20]. After filtration, the CN/TiO-CNT membrane was annealed in a flow of argon (40 sccm) at 500 °C for 2 h at a heating rate of 2 °C min^{-1}. Graphene oxide (GO) was synthesized by modified Hummers' method through oxidation of graphite powder [21]. Then GO was decorated on to the CN/TiO-CNT membranes via the filtration method to construct nanoscale channels. Briefly, 20, 40, 60, 100 and 150 mL of GO solution (5 mg L^{-1}) was filtrated stepwise on the CN/TiO-CNT membranes by the vacuum pump, denoted as GO/CN/TiO-CNT_1, GO/CN/TiO-CNT_2, GO/CN/TiO-CNT_3, GO/CN/TiO-CNT_4 and GO/CN/TiO-CNT_5 membranes, respectively. The schematic diagram of the preparation of GO/CN/TiO-CNT membranes is shown in Scheme 1.

2.2. Characterization

The morphological structure of GO/CN/TiO-CNT membrane was analyzed using scanning electron microscopy (SEM; Quanta 200 FEG) and transmission electron microscopy (TEM, FEI-Tecnai G^2 F30). The crystallinity of the sample was determined by X-ray diffractometer (XRD, EMPYREAN, PANalytical) using a diffractometer with Cu Kα radiation. The specific surface area was measured via an Automated

Surface Area and Pore Size Analyzer (Quantachrome Autosorb-1 MP) and calculated by using the Brunauer-Emmett-Teller (BET) equation. Fourier transform infrared (FT-IR) spectroscopy of the scraped sample powder was obtained in KBr pellets on a Nicolet 5DXC IR spectrometer (Nicolet, Madison). X-ray photoelectron spectroscopy (XPS, ESCALAB 250XI, Thermo Fisher Scientific) was used to analyze the elementary composition of samples. Photoluminescence (PL) spectra of the samples were measured using a fluorescence spectrometer (Hitachi F-4500). The photocurrent intensities were measured in Na_2SO_4 electrolyte (0.1 M) using the electrochemical station (CHI660D, Shanghai Chenhua Instrument Co., China) in a conventional three-electrode configuration.

2.3. Membrane performance tests

The performance of GO/CN/TiO-CNT membrane under the photo-assistance was evaluated by the flux of water, the rejection of rhodamine B (RhB, electroneutral at pH 6), methyl orange (MO, negative charge at pH 6) and, various salt solutions (Na_2SO_4, NaCl, $MgSO_4$ and $MgCl_2$, 2 g L^{-1}), the removal of bisphenol A (BPA, a typical endocrine disrupting chemical), sulfamethoxazole (SMX, a kind of widely used antibiotics), and ammonia (a notorious toxin to aquatic animals). The antifouling capability of the membranes was also investigated with humic acid (HA, 10 mg•L^{-1}). A high pressure Xe short arc lamp (CHF-XM35, Beijing Changtuo Sci-tech Co. Ltd., China) was used as a light source, providing an incident light with an intensity of 100 mW Cm^{-2}, which was measured by a radiometer (model FZ-A, Photoelectric Instrument Factory Beijing Normal University, China). The concentration of RhB was determined by measuring the optical absorption at 554 nm with a JASCO UV–vis spectrophotometer (V550, Japan). The total organic carbon was measured using a TOC analyzer (Multi N/C 2100S, Analytik-jena, Germany). The concentrations of total ammonia nitrogen (TAN), nitrite-nitrogen (NO_2-N), and nitrate-nitrogen (NO_3-N) were determined colorimetrically using a Technicon AutoAnalyzer II system (Bran + Luebbe, Buffalo Grove, IL). The concentrations of BPA and SMX were determined by high performance liquid chromatography (HPLC, Waters-2695, USA). All the NF performance evaluation was carried out in a self-designed dead-end filtration membrane module driven by a pump. The trans-membrane pressure was set in the range of 0 − 3 bar. The effective area of the membrane at the operating pressure was 12.56 cm^2. All experiments were performed at room temperature (25 °C).

3. Results and discussion

A CN/TiO-CNT nanoporous mat is employed as the photocatalytic layer for supporting the GO layer in our experiments. Compared with the traditional functional layer, CN/TiO-CNT nanoporous mat has high porosity and an interconnected pore structure, which can significantly reduce membrane mass transfer resistance and thus enhance water flux [22,23]. The SEM images of GO/CN/TiO-CNT nanoporous functional layer are shown in Fig. 1. As illuminated in Fig. 1a, a clear edge of the thin GO layer can be seen on the CN/TiO-CNT nanoporous mat. Moreover, no fragments of GO can be found on the inner nanoporous membrane, which may be due to the large lateral size of GO. Both the GO laminates and nanoporous substrate can be clearly observed, indicating successful formation of the GO layer on top of the CN/TiO-CNT nanoporous mat. The pore size of membranes can be effectively controlled from 0.48 ~ 1.71 nm by regulating GO layer thickness. Meanwhile, the increase of GO layer thickness narrowed the pores, effectively changing the physical sieving performance of GO/CN/TiO-CNT membranes (Fig. S1). The interconnected porous structure of nanoporous mat guarantees direct paths for the diffusion of water, making it an excellent supporting layer for filtration. The optical image of the GO/CN/TiO-CNT membrane is shown in the inset of Figure 1a. After drying in a vacuum, the as-made GO/CN/TiO-CNT membranes have an excellent mechanical strength with a diameter of 4.0 cm without obvious cracks.

Fig. 1b shows the SEM image with cross-sectional view of CN/TiO-CNT nanoporous mat coated on the alumina membrane support. The SEM image in Fig. 1b demonstrates that CN/TiO-CNT nanoporous mat possesses a porous, wrinkled and fluffy microstructure orderly stacked by bridging CNTs. It is also observed that the pores are highly interconnected, and the wall of pores is composed of randomly oriented g-C_3N_4 and TiO_2 nanosheets. Meanwhile, the g-C_3N_4 nanosheets are tightly attached with TiO_2 nanosheets by CNTs, forming a “sheet-CNT-sheet” structure. CN/TiO-CNT nanoporous mat also exhibits a large surface area of 152 m^2 g^{-1} (Fig. S2), which is favorable to the adsorption of contaminants. Moreover, CNTs offer a unique 1D nanochannel for water transportation and also could transfer photogenerated charge carriers from photoirradiated g-C_3N_4 to TiO_2. Herein, the CN/TiO-CNT nanoporous mat is assembled by the bridging of CNTs forming a 3D porous network, which contributes to improving the porosity of membranes (Table S2, ~86%).

The TEM image (Fig. 1c) further exhibits the well-connected porous network composed of CNTs coupling with g-C_3N_4 and TiO_2 nanosheets. It is also noteworthy that the characteristic structural features of the g-C_3N_4 and TiO_2 nanosheets bridged by CNTs are well preserved in the CN/TiO-CNT mat. The high-resolution TEM image directly shows that the lattice spacing parallel to the top and bottom facets is ~0.235 nm, corresponding to the (001) planes of anatase TiO_2 [24]. The lattice fringes of the graphitic structure of CNTs could also be clearly found in Figure 1d. In general, a good mechanical strength is beneficial for the application of membranes in practical water treatment, especially in nanofiltration. The CN/TiO-CNT membrane exhibits a good adhesion between functional layer and alumina membrane substrate after annealing (Fig. S3a).

For a composite nanofiltration membrane, the thickness of the skin layer determines the separation performance directly [25,26]. In order to better understanding of the filtration performance, GO/CN/TiO-CNT membranes with different thicknesses of GO layers are fabricated by manipulating the GO solution volume ranging from 20 to 150 mL. The thickness of the GO layer is measured on the basis of SEM images of GO/CN/TiO-CNT membranes with different GO contents (Fig. 2). The thickness of the GO layer increased with the filtrated GO solution volumes and followed a linear growth trend. The results indicate that the thickness of the GO layer can be well-controlled by simple volume manipulation.

As we know, the thickness of the skin layer has a great effect on the membrane filtration performance. Therefore, water flux of GO/CN/TiO-CNT membranes with different GO thicknesses is studied under light irradiation. As can be seen in Fig. 3a, the water flux decreased with an exponential trend under light illumination. The sharp decrease of water flux is mainly due to the increase of mass transfer resistance when the GO thickness increased. The highest water flux (16 L m^{-2} h^{-1} bar^{-1}) is obtained with light when the GO layer thickness is about 30 nm. This water flux is about 3.2 and 2.0 times higher than the values reported by the previous studies, respectively (pure water flux, 5.0 and 8.2 L m^{-2} h^{-1} bar^{-1}) [2,7]. Such a high water flux can be explained by the mechanism of photoinduced hydrophilicity reported by Wang et al. [27]. They propose that the photoinduced hydrophilicity of TiO_2 relies on the formation of surface defects upon UV light illumination. The surface of TiO_2 consists of five coordinated Ti atoms with the sixth position occupied by H_2O or OH^-. It is believed that UV irradiation creates oxygen vacancies at the two coordinated oxygen bridging sites at the surface, thereby converting Ti^{4+} ions to Ti^{3+}. These defects can in turn increase the affinity for hydroxyl ions formed by dissociation of chemisorbed water molecules and thereby forming hydrophilic domains. Meanwhile, the unique 1D nanochannel of CNTs promotes the water transporting. Hagen−Poiseuille theory further elucidates the high water flux. In this case, the distance between two adjacent GO sheets can be seen as a 2D channel between carbon walls [15,16]. The hydrophobic nature of the carbon wall in GO is also helpful for water

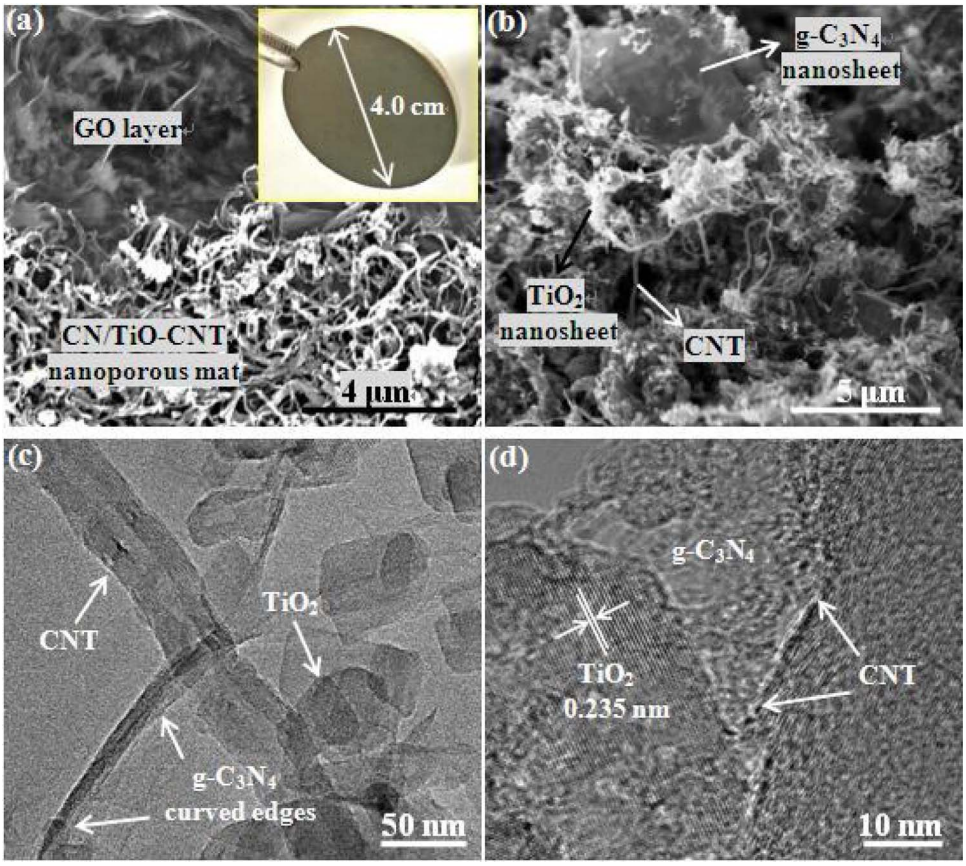

Fig. 1. (a) SEM image (top view) of GO/CN/TiO-CNT membrane (inset: digital photo). The top half of the image shows the uniform and smooth coating of GO layer, whereas the bottom half shows the porous structure of CN/TiO-CNT nanoporous mat; (b) SEM image with cross-sectional view of CN/TiO-CNT nanoporous mat coated on the alumina membrane support; (c) TEM and (d) HRTEM images of CN/TiO-CNT nanoporous mat.

transport through the slip flow theory. The water first goes to the hydrophilic "gate" (space between edges of two adjacent GO nanosheets or defects of GO) for aggregation and then slips through into hydrophobic 2D nanochannels (a conceptual illustration is shown in Scheme 2).

For the GO/CN/TiO-CNT membrane with a GO layer thickness of ~ 30 nm, the water flux increases linearly with pressure at the range of 1 − 3 bar (Fig. 3b). The results also indicate that the GO/CN/TiO-CNT membrane could resist high pressure even though the thickness of the GO layer is thin. Generally, the thin separation layer supported on the nanoporous mat cannot afford high pressure [28], whereas the GO/CN/TiO-CNT membrane presents good pressure endurance. This is mainly due to two reasons: i) the strong noncovalent π–π interactions between CNTs and GO; ii) the excellent mechanical properties of GO.

Fig. 3c presents the effect of light irradiation on pure water flux of GO/CN/TiO-CNT membranes. Benefiting from the photoinduced hydrophilicity of TiO_2, the pure water flux for the GO/CN/TiO-CNT membrane (with ~30 nm GO layer thickness) under light illumination

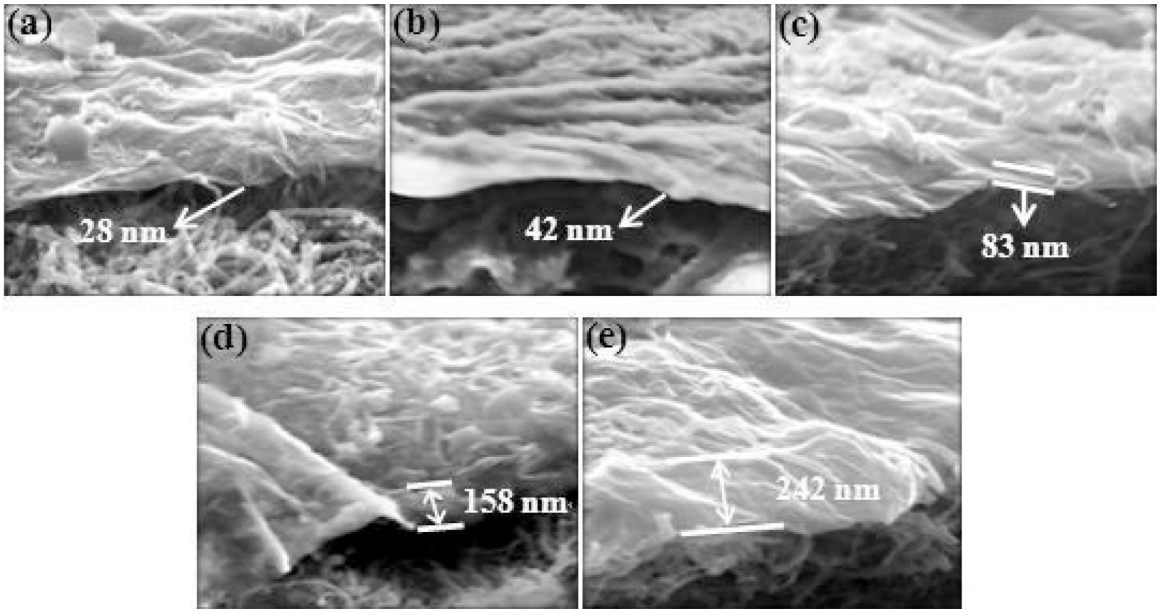

Fig. 2. Cross-section SEM images of GO/CN/TiO-CNT membranes filtrating different volume of GO solution (5 mg L^{-1}, a: 20 mL, b: 40 mL, c: 60 mL, d: 100 mL and e: 150 mL).

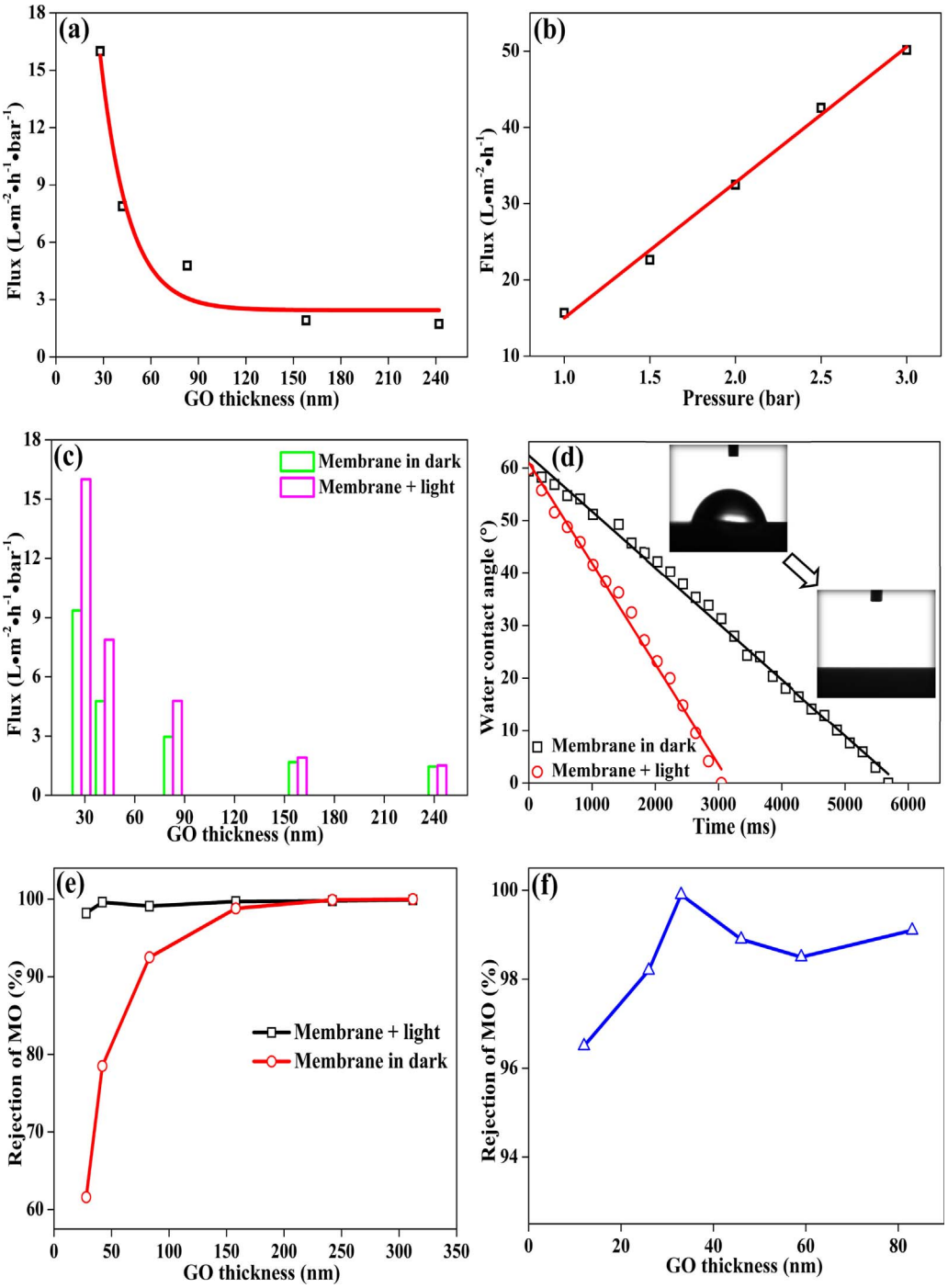

Fig. 3. (a) Relationship between pure water flux and GO layer thickness under light irradiation; (b) Water flux relative to pressure under light irradiation applied on the GO/CN/TiO-CNT membrane with a GO thickness of ~30 nm; (c) Pure water flux GO/CN/TiO-CNT membranes with and without light irradiation; (d) Water contact angle variation of GO/CN/TiO-CNT membrane (with ~30 nm GO layer thickness) with and without light irradiation; (e) and (f) Rejection of MO by GO/CN/TiO-CNT membrane with the different GO layer thickness.

is about 1.7 times higher than the same membrane without light irradiation. This indicates that the photo-assistance conduced to enhance the water flux of GO/CN/TiO-CNT membrane. However, it is also found that the increment of pure water flux gradually decreases with the increase of GO layer thickness. Obviously, once the GO layer thickness is more than 150 nm, the effect of light irradiation on the pure water flux is negligible, which could be due to the fact that too thick GO layer greatly hinders the light absorption of CN/TiO-CNT nanoporous mat.

It has been reported that UV irradiation can result in a structural change at the TiO_2 surface thereby influencing the interfacial force along the solid–liquid boundary and consequently changing the contact angle [29]. Here, water contact angle of GO/CN/TiO-CNT membrane (with ~30 nm GO layer thickness) with/without light irradiation is monitored over time by an optical contact angle & interface tension meter (SL200KB, Kino, USA). As seen from Fig. 3d, water contact angle declines over time either with or without light irradiating, which is attributed to the dynamic behavior of the sessile drops of water on GO/CN/TiO-CNT membrane. Without light irradiating, the plot of water contact angle versus time presents good linearity with a slope (absolute value) of 0.01°•ms^{-1}. However, the slope increases approximately by 2 times with light irradiation, suggesting hydrophility of GO/CN/TiO-CNT membrane is improved by the photo-assistance, which is conducive to higher flux of water.

Rejection performance of GO/CN/TiO-CNT membranes is evaluated using an anionic organic dye (Methyl Orange, MO) as a model pollutant. The results of rejection for MO without light irradiation are shown in Fig. 3e and indicated that rejection increased with the increase of the GO layer thickness. When the thickness of GO layer is ~30 nm, the

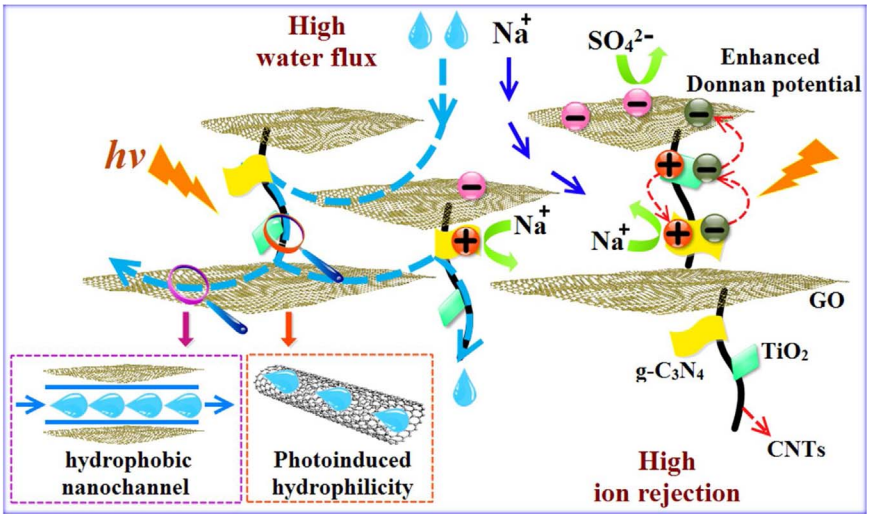

Scheme 2. Schematic diagram for illustrating the enhanced water flux and ions rejection.

rejection of MO is only 60% by the membrane filtration alone. However, approximately 100% of MO rejection is obtained as long as the GO layer thickness is more than 150 nm. The high MO rejection with GO/CN/TiO-CNT membrane separation alone is ascribed to the physical sieving and electrostatic repulsion. A previous study has reported that the size of the organic dye is bigger than the average size of the 2D nanochannels of GO [2]. Therefore, the dominant rejection mechanism is considered to be the physical sieving by 2D nanochannels formed by the space between GO nanosheets during membrane filtration alone. Meanwhile, electrostatic repulsion also contributes to the MO rejection because of the large amount of carboxylic groups at the edges of GO nanosheets [7]. Therefore, it might be necessary to obtain a high MO rejection of NF membranes via increasing the GO layer thickness and counterions on the membrane surface. However, the thick GO layer is adverse to the flux of NF membranes.

Interestingly, all the GO/CN/TiO-CNT membranes exhibit over 95% rejection of MO under light irradiation (Fig. 3e). Meanwhile, it is worth noting that the high MO rejection is also obtained even if GO layer thickness is only ~30 nm, compared with the membrane filtration alone under same GO thickness, indicating that the MO rejection could be greatly improved through the photo-assistance even with the thinner GO layer. The high MO rejection could be explained by following two reasons: i) the photogenerated electrons enrichment on GO surface under light irradiation improved the charge density per unit area, thereby resulting in the increase of MO molecules rejection in accordance with the repulsion of same charges; ii) Residual MO molecules of permeating membrane would be degraded benefiting from the photodegradation of excited g-C_3N_4 and TiO_2. It can be seen from Fig. 3f that an optimal MO rejection is obtained with ~33 nm GO layer because of the synergistic effect of photocatalysis and membrane filtration. When the GO layer thickness is less than 100 nm, the photocatalysis and membrane filtration synergistically dominated the rejection of MO. Once the GO layer thickness was more than 100 nm, the physical sieving of membranes would play a major role in the MO rejection, because the narrowed membrane pores is sufficient to reject MO molecules.

Fouling resistance ability is crucial to NF membrane applications in water treatment. Usually, the accumulation including micro-organisms, inorganic colloids or proteins from the wastewater on the membrane surface would cause the membrane fouling. Severe fouling disfavors the permeation of desired molecules, diminishes the NF performance and ultimately shortens the lifetime of the membranes. The physical and chemical characteristics of membrane surface like pore morphology, pore size, porosity and hydrophobicity-hydrophilicity strongly affect the fouling behaviour of membranes [30]. Generally, a hydrophilic surface can form a water layer, which retards the adsorption of protein and other foulants. And most foulants are adsorbed on the membrane by hydrophobic interaction. Fortunately, our membranes retain hydrophilic groups (Fig. S2, FTIR) on the surface of GO nanosheet and hydrophobic nanochannels in the interlayer space between neighbored graphene sheets [31]. In addition, the introduction of CNTs increases the hydrophily of GO/CN/TiO-CNT membrane. The antifouling performance of GO/CN/TiO-CNT membrane (with ~33 nm GO thickness) with and without light irradiation was investigated using 10 mg•L^{-1} of HA solution as foulant simulator. As presented in Fig. 4a, the membrane without light assistance shows that the water flux went through a sharp decline after HA solution was fed into the membrane module with the running time. However, a flux of HA solution markedly increases as soon as the light is switched on. This result indicates that integrating membrane separation with photo-assistance is beneficial to improve the recovery performance of the fouled membranes.

Generally, long-term filtration operation is necessary in actual water treatment. Hence, regeneration capability is one of the major concerns for membrane separation technology especially in practical applications. Herein, the stability and reusability of GO/CN/TiO-CNT membranes are also evaluated by the flux recovery (F_r), which is calculated by the following equation:

$$F_r(\%) = \left(\frac{J_{W,i} - J_{M,i}}{J_{M,i}}\right) \times 100 \quad (1)$$

where, $J_{W,i}$, $J_{M,i}$ is the flux of membrane for HA solution (10 mg L^{-1}) with and without light irradiation after cycle i, respectively. The results of flux recovery are shown in Fig. 4b. The flux recovery of treating HA solution remained almost constant (over 60%) under photo-assistance after each cycle. Two major reasons for the good stability and reusability are: i) most of electrons and holes from photocatalysts is continuously generated under light irradiation, further leading to the yield of active radicals, which are effective oxidation agents in destroying HA. The reactions of HA with active species to the generation of CO_2 and the formation of ring-opened products would contribute to a decrease in molecular size [32]; ii) the unique 1D nanochannel of CNTs for water transporting is also favorable to the fast transmission of destroyed HA, thereby mitigating membrane fouling effectively.

To visually expound the effect of photo-assistance on antifouling property of membrane, the rejection of RhB with and without light irradiation is also carried out in this work. Based on the Akbari's report [33], RhB was electroneutral at pH 6, thereby RhB molecules would be adsorbed on the GO surface and injected into the interlayer between GO nanosheets, which greatly cause the membrane fouling. Fig. 4c presents the photographs of the GO/CN/TiO-CNT membranes without and with

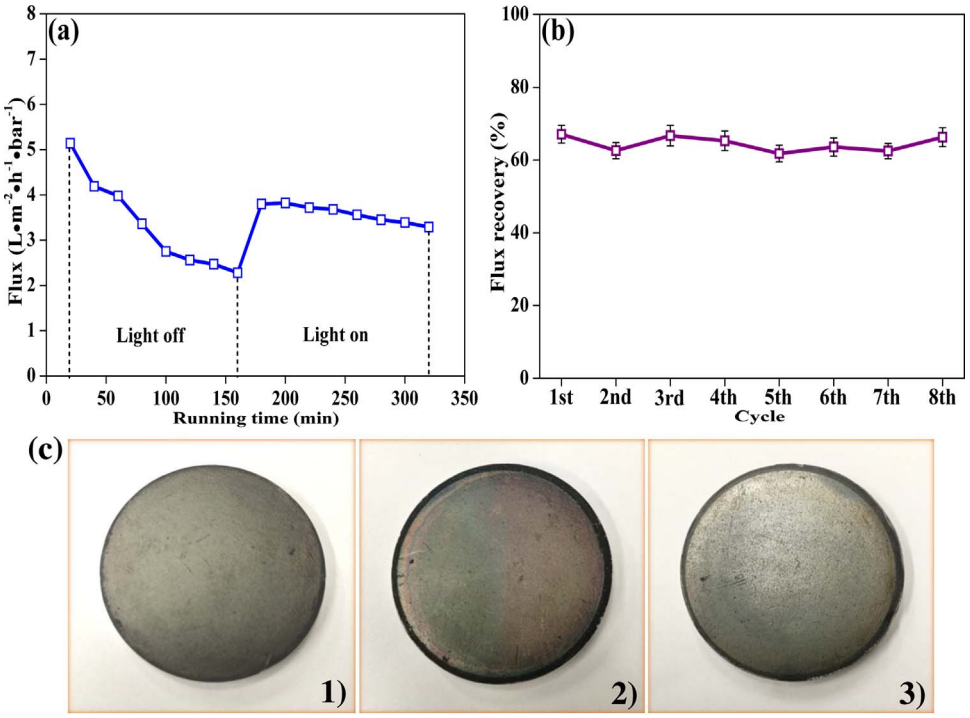

Fig. 4. (a) Antifouling tests for (a) GO/CN/TiO-CNT membrane (with ~33 nm GO layer thickness) under the 2 bar. Flux was plotted versus time for two periods: 10 mg L^{-1} of HA solution flux for first 160 min, and HA solution flux under light irradiation for next 160 min; (b) Flux recovery of GO/CN/TiO-CNT membrane during filtration of HA under photo-assistance after eight cycles; (c) Photographs of the membrane before 1) and after filtrating RhB without 2) and with 3) light irradiation which shows regeneration of the parent-membrane surface.

light irradiation after filtrating the RhB solution. Evidently, benefiting from the photodegradation of g-C_3N_4 and TiO_2, the red color of membrane surface completely disappeared under light illumination even though continuously running for six hours comparing to the membrane filtration alone.

The retention performance of salts can reflect the charge characteristics of NF membranes, so salts rejection is an important factor for NF membranes [34]. Herein, we tested the salt retentions of photo-assisted GO/CN/TiO-CNT membranes (with ~33 nm GO thickness) to four kinds of salt including NaCl, Na_2SO_4, $MgCl_2$ and $MgSO_4$ at the concentration of 2 g L^{-1} under a pressure of 2 bar. The results are shown in Fig. 5a. A high retention of Na_2SO_4 was achieved at ≈ 67% (with ~33 nm GO layer thickness) under light irradiation. This retention value of Na_2SO_4 is about 1.2 and 1.9 times higher than that of previous reports (57% of Na_2SO_4 retention with 128 nm GO layer thickness and 35% of Na_2SO_4 retention with 150 nm GO layer thickness) [6,33]. And it is worth noting that GO/CN/TiO-CNT membranes showed a high Na_2SO_4 rejection under light irradiation even at thin GO layer. The high Na_2SO_4 retention might be attributed to the increased co-ion (ions with the same charge as the membrane) concentration under photo-assistance. Besides, the retention of Na_2SO_4 is higher than NaCl, $MgSO_4$ and $MgCl_2$ under the same experimental conditions. This result can be explained by Donnan exclusion theory that is usually used to explain the retention mechanism for charged NF membranes [34]. GO/CN/TiO-CNT membranes are negatively charged due to the carboxylic groups at edges and holes of GO sheets. Based on the Donnan exclusion theory, the Donnan potential at the interphase of solution and membrane tends to exclude co-ions from the membrane. To keep the electroneutrality of the solution on each side of the membrane, the counterions (ions with opposite charge of the membrane) have to be rejected as well. Hence, the salt retention is sensitive to the valences of the cationic (z^+) and anionic (z^-) species of the salts. Donnan theory provides the following equation for the retentions (R) of different salts [2]:

$$R = 1 - \frac{c_i^m}{c_i} = 1 - \left\{ \frac{|z_i| c_i}{c_x^m + |z_i| c_i^m} \right\}^{|z_i/z_j|} \quad (2)$$

where z_i and z_j are the valence of co-ions and counterions, c_i and c_i^m are the concentrations of co-ions in the bulk solution and membrane respectively, c_x^m is the membrane charge concentration, and subscripts i and j indicate co-ions and counterions, respectively. From this equation, it can be qualitatively calculated that the retention sequence of the salts used is R (Na_2SO_4) > R (NaCl) ≈ R ($MgSO_4$) > R ($MgCl_2$). Our experimental sequence is identical with the calculated one, meaning that

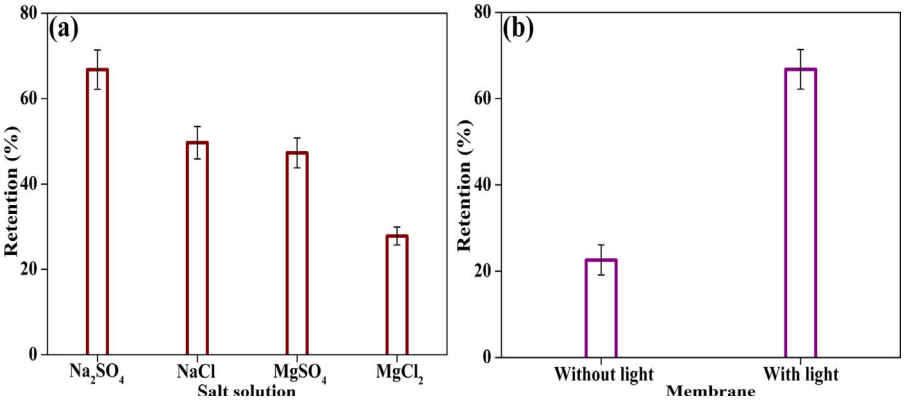

Fig. 5. (a) Retention measured for four different salt solutions (2 g L^{-1}) with different ion valences under light irradiation; (b) Retention measured for Na_2SO_4 solution (2 g L^{-1}) with and without light irradiation. The GO/CN/TiO-CNT membrane used here had a GO layer thickness of ~ 33 nm, and a pressure of 2 bar was applied.

the salt rejection of the GO/CN/TiO-CNT membrane is mainly determined by the Donnan exclusion.

To illuminate the effect of photocatalysis on improving the ions rejection, the rejection of Na_2SO_4 solution by GO/CN/TiO-CNT membrane with and without light irradiation is carried out, as shown in Fig. 5b. The retention for Na_2SO_4 is only 23% in the absence of light illumination, however, the Na_2SO_4 retention increased about 3 times with photo-assistance. Therefore, the introduction of photocatalysis technology into the NF membranes is favorable to improving the salt rejection of NF membranes. A corresponding mechanism of high water flux and high ion rejection via GO/CN/TiO-CNT membrane has been explored in Scheme 2.

Ammonia, a typical environmental contaminant, is often found in surface water and aquaculture water. It is well-known that ammonia is toxic to aquatic animals, even at low concentrations [35]. It has been demonstrated that ammonia could diffuse through the epithelial membrane of fish and could then cross the blood-brain barrier to poison the central nervous system of fish [36]. Long-term exposure to ammonia also significantly inhibits the growth of fish because of the decrease in food intake [37]. However, the conventional GO-based NF membranes cannot effectively convert the ammonia into the other inorganic nitrogen (such as nitrate-nitrogen (NO_3-N), nontoxic to fish) owing to their single separation function. Wang et al. [35] has reported that the ·OH (from electrons) and photogenerated holes could oxidize the ammonia into NO_3-N. To evaluate the performance of multifunctional NF membranes for removing ammonia, the concentrations of nitrite-nitrogen (NO_2-N) and NO_3-N are measured during the total ammonia nitrogen (TAN) treatment process using the GO/CN/TiO-CNT membranes under light irradiation. As shown in Fig. 6a, when the TAN concentration decreased from 1.53 mg L^{-1} (feed concentration) to approximately 0.76 mg L^{-1} (permeate concentration), the concentration of NO_3-N reached about 0.59 mg L^{-1} (permeate concentration). In addition, it is important to note that the product of NO_2-N only accumulated to less than 0.08 mg L^{-1} (permeate concentration), which would be beneficial for ecological safety, because NO_2-N is a toxic contaminant that threatens aquatic animals' survival and growth [38]. The yield of NO_2-N is clearly lower than that of NO_3-N, implying that the NO_3-N is the major product for the TAN photocatalytic conversion. Moreover, the calculated mass recoveries of nitrogen atoms in water indicated that the direct quantitative measurement of the N-mass of TAN, NO_2-N, and NO_3-N in the aqueous solution is in good agreement with the total nitrogen mass balance. It is noted that the removal of TAN in outlet water is slightly higher than the total of inorganic N atoms from NO_3-N and NO_2-N during the integrated process, which could be ascribed to the membrane rejection based on the Donnan exclusion. For comparison, the removal of TAN by GO/CN/TiO-CNT membrane with and without light irradiation is also carried out. The results of TAN removal are shown in Fig. 6b. Approximately 12% of TAN is rejected only through the membrane filtration alone. The rejection mechanism for TAN is perhaps mainly owing to: i) the electrostatic repulsion between negatively charged Cl^- (from NH_4Cl) and carboxylic groups of GO surface according to Donnan exclusion; ii) the large specific surface area of CNTs contributes to the adsorption of TAN. However, more than 50% of TAN is removed by the GO/CN/TiO-CNT membrane under light irradiation, which is almost 4.2 times higher than that of the membrane filtration alone. This indicates that the introduction of photocatalysis is beneficial to the TAN removal. In addition, the removal of sulfamethoxazole (about 80%) and bisphenol A (more than 80%) under light irradiation further exhibits the multifunctional characteristic of GO/CN/TiO-CNT membrane (Fig. S7 and S8).

To evaluate the practicability of the photo-assisted GO/CN/TiO-CNT membranes, we collect aquaculture water from an aquaculture pond in Dalian city. Table S3 shows the typical items of water quality for the aquaculture water. As displayed in Fig. 6c, for the membrane separation process, the removal rate of turbidity is about 90%, whereas

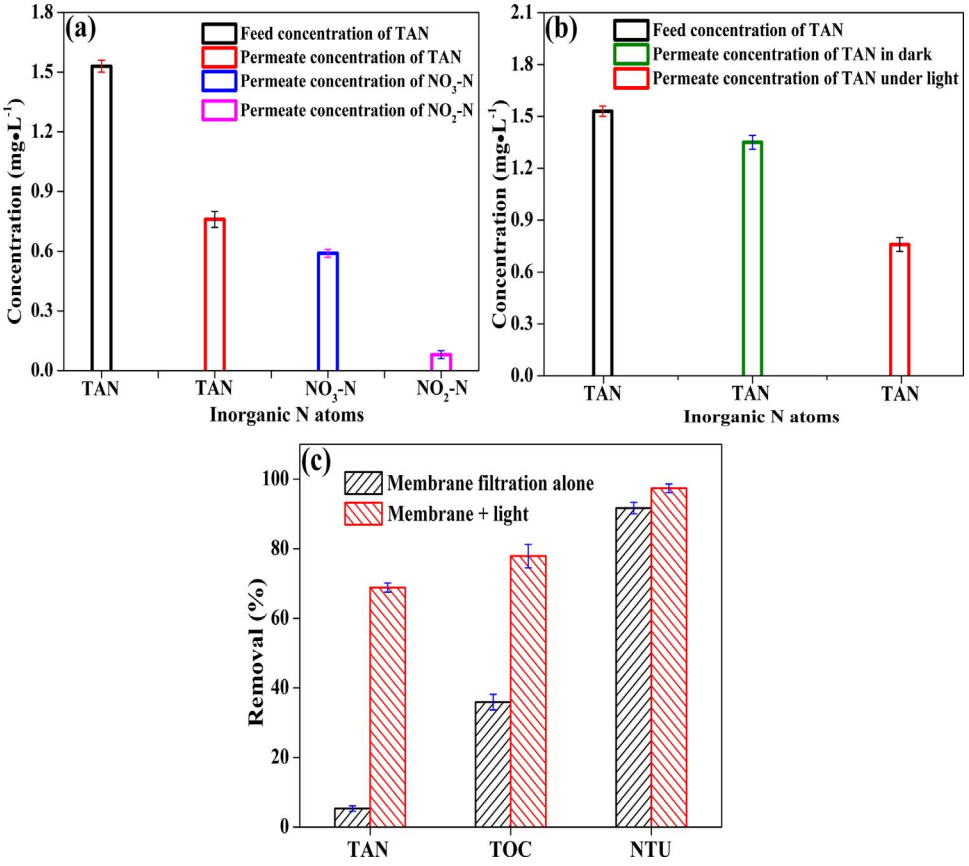

Fig. 6. (a) Variations of TAN, NO_2-N and NO_3-N concentrations by GO/CN/TiO-CNT membrane (with ~33 nm GO layer thickness) under light irradiation; (b) Comparison of the photo-assisted effect on TAN removal via GO/CN/TiO-CNT membrane with and without light; (c) The contaminants removal from real aquaculture water by GO/CN/TiO-CNT membranes.

more than 95% of the turbidity removal is obtained by the GO/CN/TiO-CNT membrane under the photo-assistance. The integrated process presents better performance on organic pollutant removal than that of membrane filtration alone due to the photocatalytic degradation of organic contaminants. Removal of TOC is only 35% for the membrane filtration alone and reached 78% for the integrated process. The removal results of ammonia are shown in Fig. 6c. About 70% of TAN removal is obtained by the GO/CN/TiO-CNT membrane under light irradiation, whereas it is less than 6% under the membrane filtration alone. Furthermore, the conversion ratio of NO_3-N is approximately 60% through the photo-assisted membrane. These results clearly manifest the excellent performance in real aquaculture water treatment for the integrating the nanofiltration and photocatalysis comparing with the membrane filtration alone.

Herein, a mechanism of photo-assisted layer-by-layer enhancing the water flux and ion rejection is hypothesized, as shown in Scheme 2. For the high water flux, previous explanation is on the basis of the following aspects: (1) the nanofibrous mat has a relatively high porosity leading to a low transport resistance; (2) the large lateral size of GO layer offers the longer hydrophobic 2D nanochannel contributing to higher speed of water at the ends of these channels [7]. In addition, the GO interlayer spacing (0.6 ~ 1 nm) is larger than the kinetic diameters of water (0.265 nm), namely, water can easily pass through the spacing [26]. The high water flux of photo-assisted GO/CN/TiO-CNT membrane mainly depends on the photoinduced hydrophilicity of TiO_2 on the surface of CNTs in the present work. Under light irradiation, the photoinduced electrons reduce the Ti sate form Ti^{4+} to Ti^{3+}, then the oxygen atoms will be ejected creating oxygen vacancies which contribute to increasing the affinity for water molecules and thus transforming the surface hydrophilic [29]. Therefore, TiO_2 nanomaterials exhibit superhydrophilicity (water-contact angle of $0^\circ \pm 1^\circ$) upon light-irradiation, which is advantageous for enhancing the water flux. Meanwhile, the unique 1D nanochannel of CNTs is beneficial to water transporting. When the incident light irradiated the surface of CN/TiO-CNT mat, benefiting from the photoinduced hydrophilicity of TiO_2 and unique structure of CNTs, more water is injected into the nanochannel of CNTs and rapidly transported as Scheme 1 showed. Hence, a high flux of GO/CN/TiO-CNT membranes is obtained under photochemical assistance owing to the enhanced water transmission via layer-by-layer sieving.

The mechanism of enhanced ion rejection depending on photoinduced charge carriers under light illumination is also shown in Scheme 2. When the light irradiates on the CN/TiO-CNT nanoporous mat, the incident light can be directly absorbed by CN/TiO-CNT and also scattered by its nanoporous framework. With the transmission of scattered light, it can be absorbed by the inner framework, leading to an enhanced light utilization. According to the CB and VB edge potentials of g-C_3N_4 and TiO_2 (−1.12 and 1.57 eV, −0.29 and 2.91 eV, respectively) [39], in the TiO_2/g-C_3N_4 heterojunctions, both TiO_2 and g-C_3N_4 can absorb light to produce photoinduced electron–hole pairs. The photoexcited electrons can jump from the VB to the CB of g-C_3N_4 and then transfer from the CB of g-C_3N_4 to that of TiO_2 under light irradiation. In addition, since the VB edge potential of TiO_2 is more positive than that of g-C_3N_4, the holes at the VB of TiO_2 can transfer to the VB of g-C_3N_4. However, the transmission of photogenerated electrons in heterojunctions contributes to reducing the recombination of electron–hole pairs and prolonging the charge lifetime, then leaves more electrons in the CB of TiO_2 and more holes in the VB of g-C_3N_4 [40]. Subsequently, photoexcited electrons would migrate and transfer to GO surface due to the favorable equilibrium Fermi level positions, as shown in Scheme 2 [41,42]. Hence, the abundant negative charges including enthetic photogenerated electrons and inherent various negatively charged oxygen functional groups are aggregated on the surface of GO layer, and the photoinduced holes (positively charged) are remained in the VB of g-C_3N_4 under light irradiation [19]. The surface charge density of membrane is about 29.7 $C{\cdot}m^{-2}$ under the photo-assistance, which is almost 2 times higher than the membrane without light irradiation (Fig. S6b). The increase of surface charge density of membrane under light irradiation further proves the hypothesis. According to Donnan exclusion, the ionic concentrations at the membrane surface are not equal to those in the bulk solution. The counterion (ions with opposite charge of the membrane) concentration is higher at the membrane surface compared to that of the bulk solution. Co-ion (ions with the same charge as the membrane) concentration is lower at the membrane surface. When an external pressure is applied on the membrane, water can pass through the membrane, whereas co-ions are rejected owing to the Donnan potential. Meanwhile, counterions are also rejected because of the requirements of electroneutrality. Herein, the GO layer exhibits preferential sorption of water [26], causing water molecules to gather on the surface of the GO membrane and impede other molecules. Subsequently, the water diffuses fast in the interlayer spacing due to the low-friction flow of water [43]. Most of negative ions in water are rejected because the GO surface aggregates abundant same charges under light irradiation, meanwhile, a part of positive ions are also retained to maintain the electroneutrality. Moreover, residuary positive ions permeating the GO layer would be further rejected owing to the remained positive charges (photogenerated holes) in the VB of g-C_3N_4. Thus, a multifunctional NF membrane with the layer-by-layer rejecting the counterions is constructed under the photo-assistance.

4. Conclusion

The GO/CN/TiO-CNT membrane with both high flux ($16\ L\ m^{-2}\ h^{-1}\ bar^{-1}$) and high ions rejection (67%) is successfully constructed by coupling the photocatalysis with NF membrane separation for the first time. The multifunctional characteristics are also exhibited by the efficient removal of TAN (50%), SMX (80%) and BPA (82%) under light irradiation. The treatment of real aquaculture water further indicates its excellent practical application ability. In addition, the GO/CN/TiO-CNT membrane also shows a good regeneration capability and stabilized long-term filtration operation due to the photo-assistance. Its high water flux and high salt rejection is based on the Donnan exclusion and layer-by-layer sieving under the photo-assistance. This work proves that introducing the photocatalysis technology into the GO-based NF membrane could be an effective strategy for constructing advanced next-generation GO-based NF membranes in the water treatment.

Acknowledgements

This work was supported by National Natural Science Foundation of China (51478075), the Program of Introducing Talents of Discipline to Universities (B13012), programme for Changjiang Scholars and Innovative Research Team in University (IRT_13R05). and the Fundamental Research Funds for the Central Universities (DUT16TD02).

Appendix A. Supplementary data

Supplementary data associated with this article can be found, in the online version, at http://dx.doi.org/10.1016/j.apcatb.2017.10.016.

References

[1] M.A. Shannon, P.W. Bohn, M. Elimelech, J.G. Georgiadis, B.J. Marinas, A.M. Mayes, Nature 452 (2008) 301–310.
[2] Y. Han, Z. Xu, C. Gao, Adv. Funct. Mater. 23 (2013) 3693–3700.
[3] R.K. Joshi, P. Carbone, F.C. Wang, V.G. Kravets, Y. Su, I.V. Grigorieva, H.A. Wu, A.K. Geim, R.R. Nair, Science 343 (2014) 752–754.
[4] X.L. Xu, F.W. Lin, Y. Du, X. Zhang, J. Wu, Z.K. Xu, ACS Appl Mater. Inter. 8 (2016) 12588–12593.
[5] X.F. Fan, H.M. Zhao, Y.M. Liu, X. Quan, H.T. Yu, S. Chen, Environ. Sci. Technol. 49 (2015) 2293–2300.
[6] L. Hu, S.J. Gao, X.G. Ding, D. Wang, J. Jiang, J. Jin, L. Jiang, ACS Nano 9 (2015) 4835–4842.

[7] J. Wang, P. Zhang, B. Liang, Y. Liu, T. Xu, L. Wang, B. Cao, K. Pan, ACS Appl. Mater. Inter. 8 (2016) 6211–6218.
[8] Y. Lv, C. Zhang, A. He, S.J. Yang, G.P. Wu, S.B. Darling, Z.K. Xu, Adv. Funct. Mater. 27 (2017) 1700251.
[9] H.X. Zhao, S. Chen, X. Quan, H.T. Yu, H.M. Zhao, Appl. Catal. B-Environ. 194 (2016) 134–140.
[10] D.K. Wang, M. Elma, J. Motuzas, W.C. Hou, F.W. Xie, X.W. Zhang, J. Membrane Sci. 524 (2017) 163–173.
[11] X.F. Qian, M. Ren, D.T. Yue, Y. Zhu, Y. Han, Z.F. Bian, Y.X. Zhao, Appl. Catal. B-Environ. 212 (2017) 1–6.
[12] X.F. Qian, D.T. Yue, Z.Y. Tian, M. Reng, Y. Zhu, M. Kan, T.Y. Zhang, Y.X. Zhao, Appl. Catal. B-Environ. 193 (2016) 16–21.
[13] R. Wang, K. Hashimoto, A. Fujishima, M. Chikuni, E. Kojima, A. Kitamura, M. Shimohigoshi, T. Watanabe, Nature 388 (1997) 431–432.
[14] J. Schaep, B. Van der Bruggen, C. Vandecasteele, D. Wilms, Sep. Purif. Technol. 14 (1998) 155–162.
[15] G. Hummer, J.C. Rasaiah, J.P. Noworyta, Nature 414 (2001) 188–190.
[16] K. Falk, F. Sedlmeier, L. Joly, R.R. Netz, L. Bocquet, Nano Lett. 10 (2010) 4067–4073.
[17] M. Majumder, N. Chopra, B.J. Hinds, ACS Nano 5 (2011) 3867–3877.
[18] I. Robel, B.A. Bunker, P.V. Kamat, Adv. Mater. 17 (2005) 2458–2463.
[19] A. Kongkanand, P.V. Kamat, ACS Nano 1 (2007) 13–21.
[20] X. Zhang, D.K. Wang, D.R.S. Lopez, J.C. Diniz da Costa, Chem. Eng. J. 236 (2014) 314–322.
[21] W.S. Hummers, R.E. Offeman, J. Am. Chem. Soc. 80 (1958) 1339.
[22] K. Yoon, K. Kim, X. Wang, D. Fang, B.S. Hsiao, B. Chu, Polymer 47 (2006) 2434–2441.
[23] T.M. Yeh, Z. Wang, D. Mahajan, B.S. Hsiao, B. Chu, J. Mater. Chem. A 1 (2013) 12998–13003.
[24] Y.J. Yuan, Z.J. Ye, H.W. Lu, B. Hu, Y.H. Li, D.Q. Chen, J.S. Zhong, Z.T. Yu, Z.G. Zou, ACS Catal. 6 (2016) 532–541.
[25] J. Wei, C. Qiu, Y.N. Wang, R. Wang, C.Y. Tang, J. Membrane Sci. 427 (2013) 460–471.
[26] K. Huang, G. Liu, Y. Lou, Z. Dong, J. Shen, W. Jin, Angew. Chem. Int. Edit. 53 (2014) 6929–6932.
[27] R. Wang, K. Hashimoto, A. Fujishima, M. Chikuni, E. Kojima, A. Kitamura, M. Shimohigoshi, T. Watanabe, Nature 388 (1997) 431–432.
[28] M. Tian, R. Wang, K. Goh, Y. Liao, A.G. Fane, J. Membrane Sci. 486 (2015) 151–160.
[29] S. Banerjee, D.D. Dionysiou, S.C. Pillai, Appl. Catal. B-Environ. 176 (2015) 396–428.
[30] P. van der Marel, A. Zwijnenburg, A. Kemperman, M. Wessling, H. Temmink, W. van der Meer, J. Membrane Sci. 348 (2010) 66–74.
[31] T. Barroso, M. Temtem, T. Casimiro, A. Aguiar-Ricardo, J. Supercrit. Fluid. 56 (2011) 312–321.
[32] G. Xue, H. Liu, Q. Chen, C. Hills, M. Tyrer, F. Innocent, J. Hazard. Mater. 186 (2011) 765–772.
[33] A. Akbari, P. Sheath, S.T. Martin, D.B. Shinde, M. Shaibani, P.C. Banerjee, R. Tkacz, D. Bhattacharyya, M. Majumder, Nat. Commun. 7 (2016) 10891.
[34] J.M.M. Peeters, M.H.V. Mulder, H. Strathmann, J. Membrane Sci. 145 (1998) 199–209.
[35] H. Wang, Y. Su, H. Zhao, H. Yu, S. Chen, Y. Zhang, X. Quan, Environ. Sci. Technol. 48 (2014) 11984–11990.
[36] P.J. Boudreaux, A.M. Ferrara, Q.C. Fontenot, J. World Aquacult.e Soc. 38 (2007) 322–325.
[37] H. Sun, K. Lu, E.J. Minter, Y. Chen, Z. Yang, D.J. Montagnes, J. Hazard. Mater. 221 (2012) 213–219.
[38] J.A. Camargo, A. Alonso, A. Salamanca, Chemosphere 58 (2005) 1255–1267.
[39] X.C. Wang, K. Maeda, A. Thomas, K. Takanabe, G. Xin, J.M. Carlsson, K. Domen, M. Antonietti, Nat. Mater. 8 (2009) 76–80.
[40] X. Zhou, B. Jin, L. Li, F. Peng, H. Wang, H. Yu, Y. Fang, J. Mater. Chem. 22 (2012) 17900–17905.
[41] L.L. Tan, W.J. Ong, S.P. Chai, B.T. Goh, A.R. Mohamed, Appl. Catal. B-Environ. 179 (2015) 160–170.
[42] Z. Tong, D. Yang, J. Shi, Y. Nan, Y. Sun, Z. Jiang, ACS Appl Mater. Inter. 7 (2015) 25693–25701.
[43] R.R. Nair, H.A. Wu, P.N. Jayaram, I.V. Grigorieva, A.K. Geim, Science 335 (2012) 442–444.